OPEN ACCESS
IOP Publishing | IMMT
International Journal of Extreme Manufacturing
Int. J. Extrem. Manuf. 4 (2022) 032003 (15pp)
https://doi.org/10.1088/2631-7990/ac670b

Topical Review

Ultrafast synthetic strategies under extreme heating conditions toward single-atom catalysts

Guanchao He, Minmin Yan, Haisheng Gong, Huilong Fei* and Shuangyin Wang*

State Key Laboratory for Chemo/Biosensing and Chemometrics, Advanced Catalytic Engineering Research Centre of the Ministry of Education, and College of Chemistry and Chemical Engineering, Hunan University, Changsha 410082, People's Republic of China

E-mail: hlfei@hnu.edu.cn and shuangyinwang@hnu.edu.cn

Received 27 January 2022, revised 14 March 2022
Accepted for publication 11 April 2022
Published 29 April 2022

Abstract

Dispersing atomic metals on substrates provides an ideal method to maximize metal utilization efficiency, which is important for the production of cost-effective catalysts and the atomic-level control of the electronic structure. However, due to the high surface energy, individual single atoms tend to migrate and aggregate into nanoparticles during preparation and catalytic operation. In the past few years, various synthetic strategies based on ultrafast thermal activation toward the effective preparation of single-atom catalysts (SACs) have emerged, which could effectively solve the aggregation issue. Here, we highlight and summarize the latest developments in various ultrafast synthetic strategy with rapid energy input by heating shockwave and instant quenching for the synthesis of SACs, including Joule heating, microwave heating, solid-phase laser irradiation, flame-assisted method, arc-discharge method and so on, with special emphasis on how to achieve the uniform dispersion of single metal atoms at high metal loadings as well as the suitability for scalable production. Finally, we point out the advantages and disadvantages of the ultrafast heating strategies as well as the trends and challenges of future developments.

Keywords: ultrafast synthesis, single atom catalysts, extreme conditions, Joule heating, microwave heating, laser irradiation

1. Introduction

Heterogeneous catalysis plays a significant role in modern industrial processes, where the catalytic processes usually occur on the surface of a solid catalyst and the internal species have negligible effects [1–3]. Consequently, extensive research efforts have been devoted to improving the performance of heterogeneous catalysts by increasing the surface area to volume ratio of the catalyst [3, 4]. Accordingly, a simple and convenient method is to diminish the size of the metal particles to an extreme point where the metals would be reduced to isolated single atoms [1, 5–7]. Additionally, it can be expected that when the nanoparticle size decreases to the single atom level, the metal-substrate interactions would be maximized, exposing abundant defects and active sites and changing molecular orbital energy levels that may bring about special catalytic mechanisms including new reaction pathways of electron

* Authors to whom any correspondence should be addressed.

2631-7990/22/032003+15$33.00

transfer or interactions with reactants/intermediates/products, further leading to enhanced catalytic performances [8–15].

Single-atom catalysts (SACs), with individually dispersed single atoms anchored on solid supports, are currently one of the most important catalytic materials and represent new frontiers in catalysis science due to their maximum atom utilization efficiency, unsaturated coordination metal centers, quantum size effects and strong metal-support interactions [2, 4, 16–19]. However, the surface energy of metals increases to a large extent with the decrease of particle size, making individual atoms tend to agglomerate or sinter to form clusters or nanoparticles during either synthesis or operation at high temperatures [3]. It is well known that nanoparticles sinter via two mechanisms: particle migration and coalescence (PMC) and Ostwald ripening (OR) [20]. PMC is associated with particles moving on the surface of the support in a manner like Brownian motion, followed by subsequent coalescence that leads to the growth of nanoparticles. In comparison, OR involves the migration of adsorbed atoms or mobile molecular species, which is driven by the difference in free energy on the surface of the carrier and the concentration of local adsorbed atoms [20–23]. As sintering is typically undesirable in catalysts, extensive research efforts have been devoted to strengthening the interaction between the metal and the support and reducing the collapse of the substrate to prevent the sintering of metal atoms [24–27]. Up to now, various synthetic approaches have been developed to achieve uniform dispersion of metal atoms in SACs. For example, physical and chemical deposition, such as atomic-layer deposition and chemical vapor deposition, with advantages of precise control of the structure and purity of the materials, were demonstrated to afford ideal model catalysts for the fundamental research of the metal-support interaction in SACs [8, 28–30]. However, the as-involved high vacuum conditions are difficult for large-scale production due to the low yield and the complicated or expensive equipment [28]. Alternatively, a variety of wet-chemical synthetic methods, including co-precipitation [31], impregnation [6], acid leaching [32], and de-alloying [6], were employed for the synthesis of SACs, but their applicability is limited for the poor universality, complexity, long processing time and high post-processing cost [28]. Additionally, numerous research works have demonstrated that high-temperature (HT) pyrolysis is critical for single-atom stabilization and dispersion as it provides sufficient activation energy to promote the formation of bonds between metal atoms and the substrate and accelerate the atom dispersion process [25, 26, 33–35]. Up to now, HT pyrolysis is the most widely adopted method for synthesizing SACs due to its simplicity, inexpensive processing, and scalability. However, the production of nanoscale or atomic-scale catalysts is often troubled by undesired thermal diffusion, particle aggregation, or phase segregation, resulting in a gradual loss of activity due to OR during a long time (minutes to hours) treatment at high temperature [24, 36]. These drawbacks seriously hinder further developments and their potential applications, especially at the industrial level [16, 37–42].

Ultrafast pyrolysis with rapid energy input by heating shockwave and instant quenching provides great opportunities

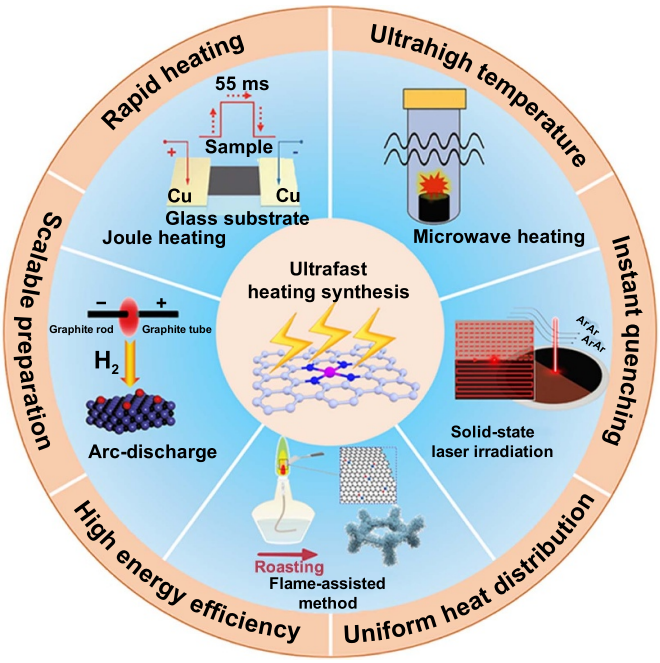

Figure 1. Overview of the main ultrafast pyrolysis synthetic methods for SACs.

to overcome the above-mentioned issues and is promised to produce SACs in a scalable and cost-effective manner [24, 26, 43]. Specifically, the ultrashort thermal shock innovatively utilizes high temperatures to synthesize SACs while the heating period is kept so short as to avoid the metal atom aggregation and destruction of the substrates, thereby maintaining the stability of the single-atom dispersion. As schematically shown in figure 1, different ultrashort thermal shock methods have been developed for the synthesis of SACs, including microwave heating [44–50], Joule heating [26, 51–55], laser heating [28] and so on. The ultrafast thermal shock processes provide several unique characteristics that are not possible with the conventional prolonged heating treatment: (a) fast ignition, rapid heating, ultrahigh transient temperature and instant quenching process to hinder the atom diffusion and agglomeration; (b) induction heating that ensures the uniform heat distribution throughout the whole material; (c) high energy efficiency and high cost-effectiveness for controllable and scalable manufacturing. These combined characteristics make the ultrafast thermal shock processes highly attractive for the rapid and facile preparation and processing of SACs, and great progress has been made within the last five years (figure 2) [26, 28, 44, 46, 50–52, 55–57]. In this review, we first summarize various ultrafast heating strategies used for the preparation of SACs, including Joule heating, microwave heating, solid-phase laser irradiation, flame-assisted method, arc-discharge method and so on, with special focus on how to achieve the uniform dispersion of single metal atoms at high metal loadings as well as the suitability for scalable production. The influences of synthetic processes and parameters on the atomic structure, catalytic activity and stability of SACs are also discussed. Finally, we point out the advantages and disadvantages of the ultrafast

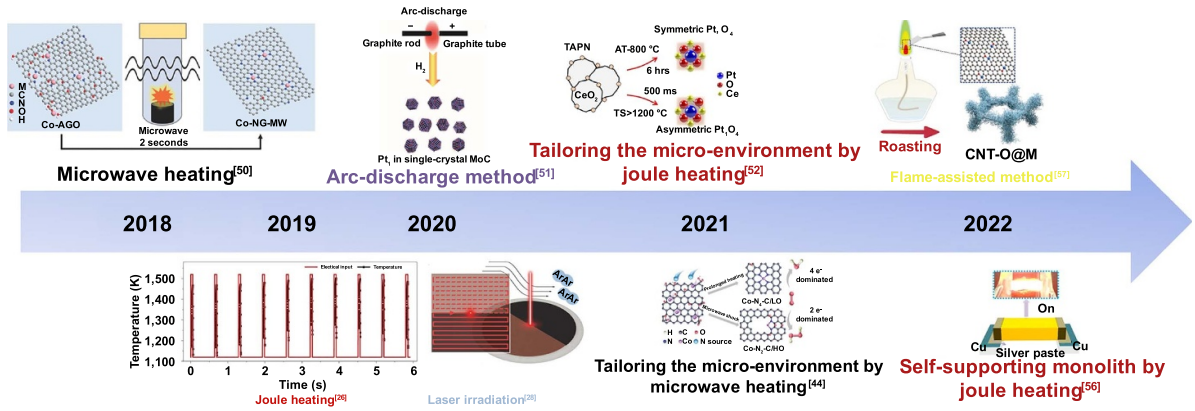

Figure 2. A brief timeline of the developments of ultrafast heating strategies for the synthesis of SACs.

heating strategies as well as the trends and challenges of future developments.

2. Joule heating

During the Joule heating, current is passed through a slightly conductive compacted powder or film and heat is generated internally due to the presence of resistance [58]. Heat is converted from the electrical energy, which is calculated by Joule's law: $Q = I^2Rt$, where I is the current value, R represents conductor resistance, and t represents the electrified time. In this case, heat can be used to synthesize nanomaterials *in situ* with ultrafast reaction rate on the conductive substrates. The rapid heating and quenching rates of Joule heating could limit the phase separation or the atom diffusion and agglomeration during synthesis and afford extremely high temperatures to form strong interaction between the metal atoms and the substrate. Joule heating has been researched for many decades but has only recently been applied to the synthesis of ultrafine nanoparticles [59, 60], high-entropy alloys [43], and SACs [25, 52, 53, 55, 61–63].

Joule heating was first used in 2019 by Yao and colleagues to synthesize SACs by repeatedly turning on/off the HT shockwaves [26]. As shown in figures 3(a)–(c), the method was to quickly heat Pt precursor on a catalyst substrate (e.g. carbon nanofiber) to high temperature up to 2000 K within a short time period (milliseconds) by Joule heating in an inert atmosphere, followed by rapid quenching (10^5 K s^{-1}). The on-state provides sufficient activation energy to form a thermodynamically stable state to ensure the atomic dispersion, while the off-state is crucial to ensure the stability of the atomic sites and the substrate. This study demonstrated that pure carbon materials were able to capture mobile atoms when nanoparticles were processed within an inert gas atmosphere at ultrahigh temperatures (1500–2000 K). While a large number of works reported that the heat treatment of the catalyst would lead to the sintering of the material and the growth of nanoparticles [3, 22, 64–66], the repeated on/off high temperature shockwaves in this work suggested that the process could be reversed and nanoparticles could be transformed into stably dispersed individual atoms [25]. Figures 3(d) and (e) show the high-angle annular dark-field scanning transmission electron microscopy (HAADF-STEM) images of Pt atoms dispersed on the support after one and ten heat shocks at a temperature of 1500 K. Under a single thermal shock, the substrate surface was distributed with a high density of individual atoms, although Pt nanoclusters were also observed. However, after ten heat shocks, the catalyst exhibited a nearly uniform distribution of single atoms, which indicates the stability of these HT-synthesized single atoms (SAs) and the further decomposition of the clusters into individual atoms during repeated shockwave heating. To further verify that Pt atoms were uniformly dispersed on the substrate, extended x-ray absorption fine structure (EXAFS) measurements were performed (figure 3(f)). The EXAFS curve of the sample with one heat shock displays a weak peak around 2.5 Å ascribed to the Pt–Pt bonding and a dominant peak around 1.5 Å assigned to the Pt–C bond, verifying the co-existence of Pt clusters and atoms. After ten heat shocks, the spectrum exhibited only one dominant peak at ∼1.5 Å for Pt–C bonds, indicating the exclusive presence of atomically dispersed Pt atoms. The resulting HT-SAs exhibited excellent activity and hydrothermal stability after steam treatment at 973 K (figure 3(g)). At the same time, due to its simplicity, Joule heating has the potential to produce SACs in a scalable manner. As a demonstration, the researchers introduced a roll-to-roll system embedded with Joule heating sources and prepared graphene-based SACs in batches. As shown in figure 3(h), the roll-to-roll preparation system consists of three parts: precursor-supplying, heat-feeding, and SAC-collecting. The preparation system removed the use of electrodes during Joule heating, enabling continuous manufacturing with improved scalability. This production process can be further simplified by streamlined manufacturing and integrating automatic parts, where all the loading, heating, and collection processes can be integrated into a single production line. The Joule heating method is ultrafast, simple, and versatile that different metal atoms (e.g. Pt, Ni, Co) can be stabilized on various substrates such as carbon, CeO_2 and C_3N_4 [20, 26, 52, 55, 56].

Following the above work, researchers have undertaken extensive studies on the preparation of SACs by repeatedly turning on/off the Joule heating shockwaves and paid special attention to the metal coordination configuration of the

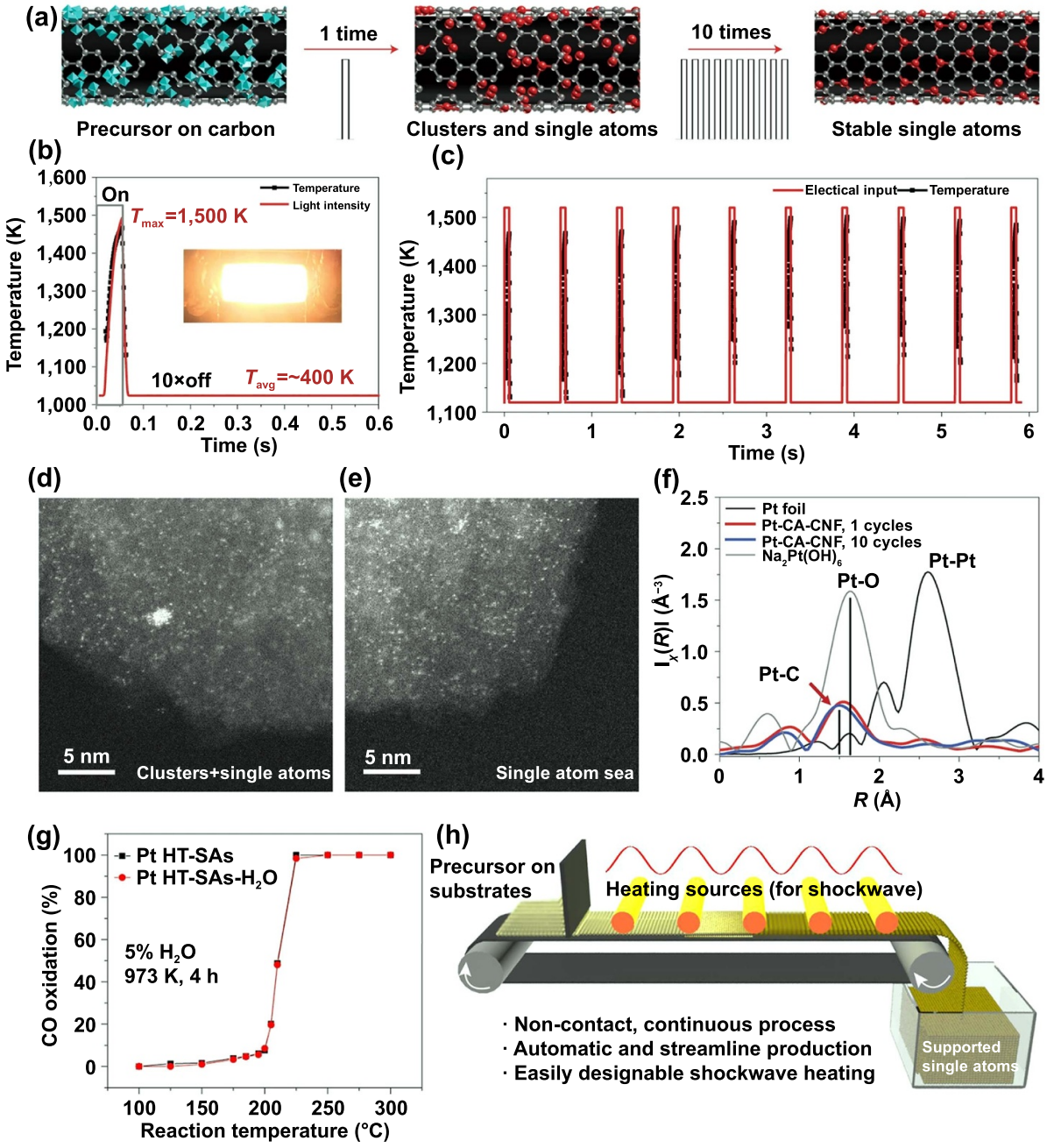

Figure 3. (a) Schematic diagram of the transformation of nanoparticles to single atoms by repeatedly on/off the high-temperature shockwaves. (b) Temperature variation and a detailed heating/quenching pattern during the pulse heat. Inset: Snapshots of the material at high temperatures. (c) Temperature profile with a ten-pulse shock heating. HAADF-STEM image of the sample after one (d) and ten (e) cycles of the heat shock. (f) EXAFS profiles of Pt HT-SAs after one and ten cycles of the heat shock treatment (without phase correction). (g) Catalytic performance of Pt HT-SAs before and after steam treatment at 973 K for 4 h. (h) Schematic for scaling up the production of single atoms using Joule heating in an automated and streamlined process. Reproduced from [26], with permission from Springer Nature.

as-synthesized SACs [52, 53, 55]. For example, Jiang and colleagues used six repeated HT thermal shocks (up to 1500 K, on-state 500 ms) to prepare Pt_1/CeO_2 SAC (Pt_1/CeO_2_TS) with high metal loading level (1 wt%) [52]. Pt_1/CeO_2_TS has a unique asymmetric structure, which is different from the symmetric and most thermodynamically stable structure prepared by traditional atom trapping methods (Pt_1/CeO_2_AT) (figure 4(a)). The HT shockwave drove the Pt dispersion by reconstructing the CeO_2 surface with the formation of strong Pt–O–Ce bond, while the rapid quenching (ca. 10^4 K s^{-1}) off-state prevented the sintering of CeO_2 and Pt. When used as catalysts for CO oxidation, Pt_1/CeO_2_TS exhibited a significantly enhanced activity and good cycling stability at low temperature, as shown in figure 4(b). In contrast, Pt_1/CeO_2_AT was rapidly deactivated due to its easy oxidation at temperature >400 °C. Hence, Pt_1/CeO_2_TS has the potential to exhibit

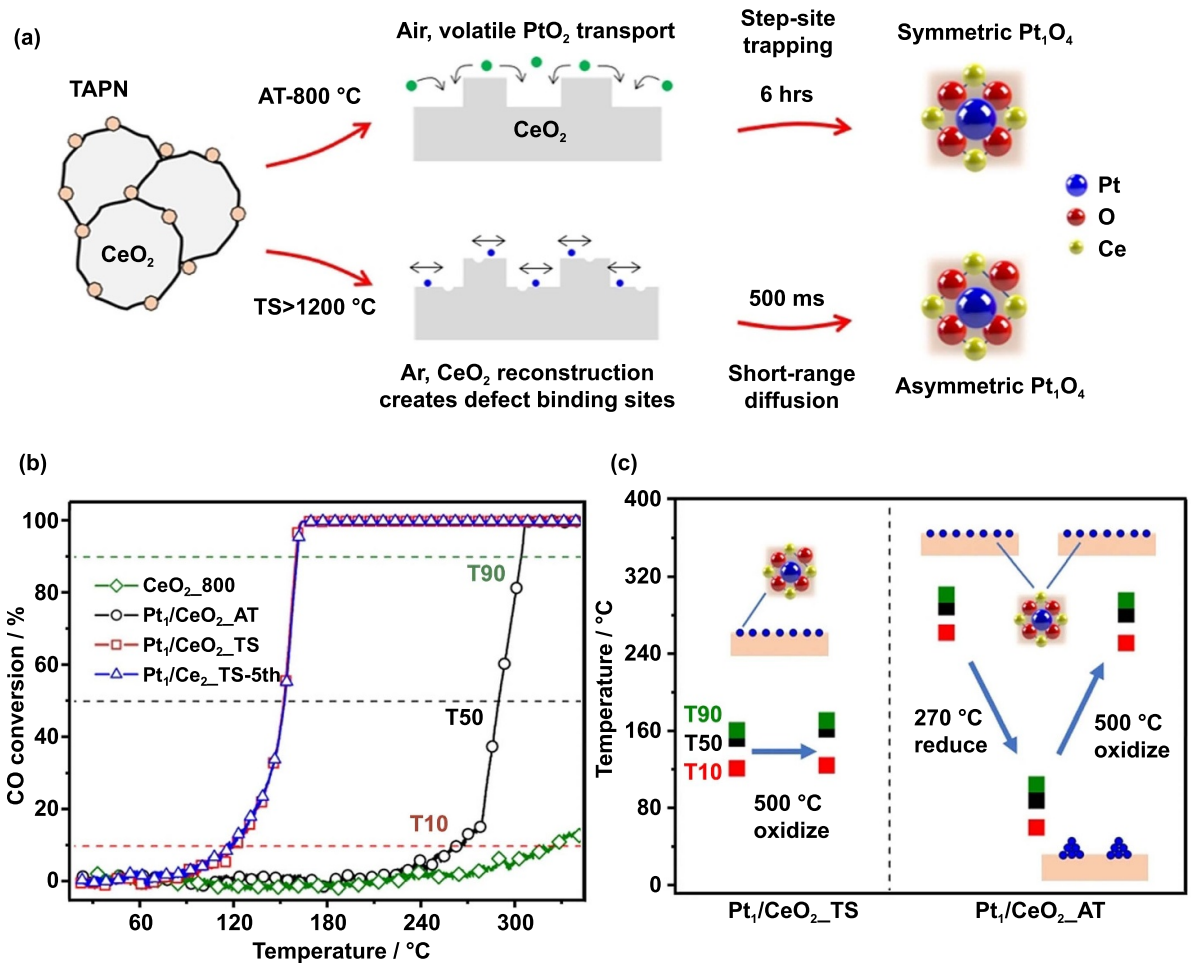

Figure 4. (a) Schematic illustration of preparation route to individually dispersed Pt atoms with different structures by the AT and TS method. (b) CO conversion of Pt_1/CeO_2_AT, Pt_1/CeO_2_TS, and CeO_2_800. (c) The T_{10}, T_{50}, and T_{90} temperatures (CO conversion rate up to 10%, 50%, and 90% of the required temperatures) of Pt_1/CeO_2_TS and Pt_1/CeO_2_AT catalysts after reductive and oxidative treatment [52] John Wiley & Sons. © 2021 Wiley-VCH GmbH.

excellent CO oxidation catalytic performance at low temperatures while being resistant to activity loss under oxidative conditions (figure 4(c)).

More recently, Xi and colleagues prepared SAC of metal- and nitrogen-doped nanocarbons (M–N–Cs) by Joule heating at a high temperature of 1300 °C within 0.5 s of HT shockwave and repeated 5 times under the protection of Ar flow to achieve the controllable doping of nitrogen species [55]. The mechanism of the catalyst formation process was illustrated in figure 5(a). Briefly, the process of preparing M–N–Cs by the Joule heating method was divided into two main steps. Firstly, Ni–N_x radicals produced by evaporating N and Ni precursors were trapped by the defects on the carbon black substrates. Then, the thermodynamically unstable metal-free N species were dissociated under high temperature. By choosing $Ni(OAc)_2$ and 1,10-phenanthroline as precursors, most of the remained N elements (up to 80%) in the resulting material were coordinated with the Ni atoms, which reduced the amounts of unfavourable uncoordinated N species in the Ni–N–C SAC (figure 5(b)), leading to high catalytic selectivity towards the CO_2 reduction reaction (CO_2RR) (figure 5(c)). In contrast, SACs prepared by traditional methods contained excessive N dopants, which inevitably interfere with the catalytic process and generate various adverse effects. Specifically, the presence of abundant unfavorable N species, especially graphitic N or pyridinic N, stimulated the competitive reaction of the HER at a relatively negative potential [67, 68], thereby inhibiting the CO_2RR selectivity of the Ni SAC (figure 5(c)).

As it is well established that in the process of preparing electrodes for electrocatalytic measurements, powder catalysts will inevitably introduce polymer binders, which could hinder mass transport and impede the exposure of active sites, resulting in unsatisfactory performance [69, 70]. For this reason, constructing a self-supporting monolithic electrode can avoid the problems encountered by traditional slurry-based electrodes [71–73]. Fei and colleagues employed the Joule heating strategy to synthesize a hierarchically porous M–N–C monolithic electrode [56]. As shown in figure 6(a), the Co^{2+}-containing amine-functionalized graphene oxide (AGO) film obtained by hydrothermal self-assembly and freeze-drying process was subjected to a HT Joule heating process for 2 s in NH_3 to acquire the Co–N–C sites integrated into

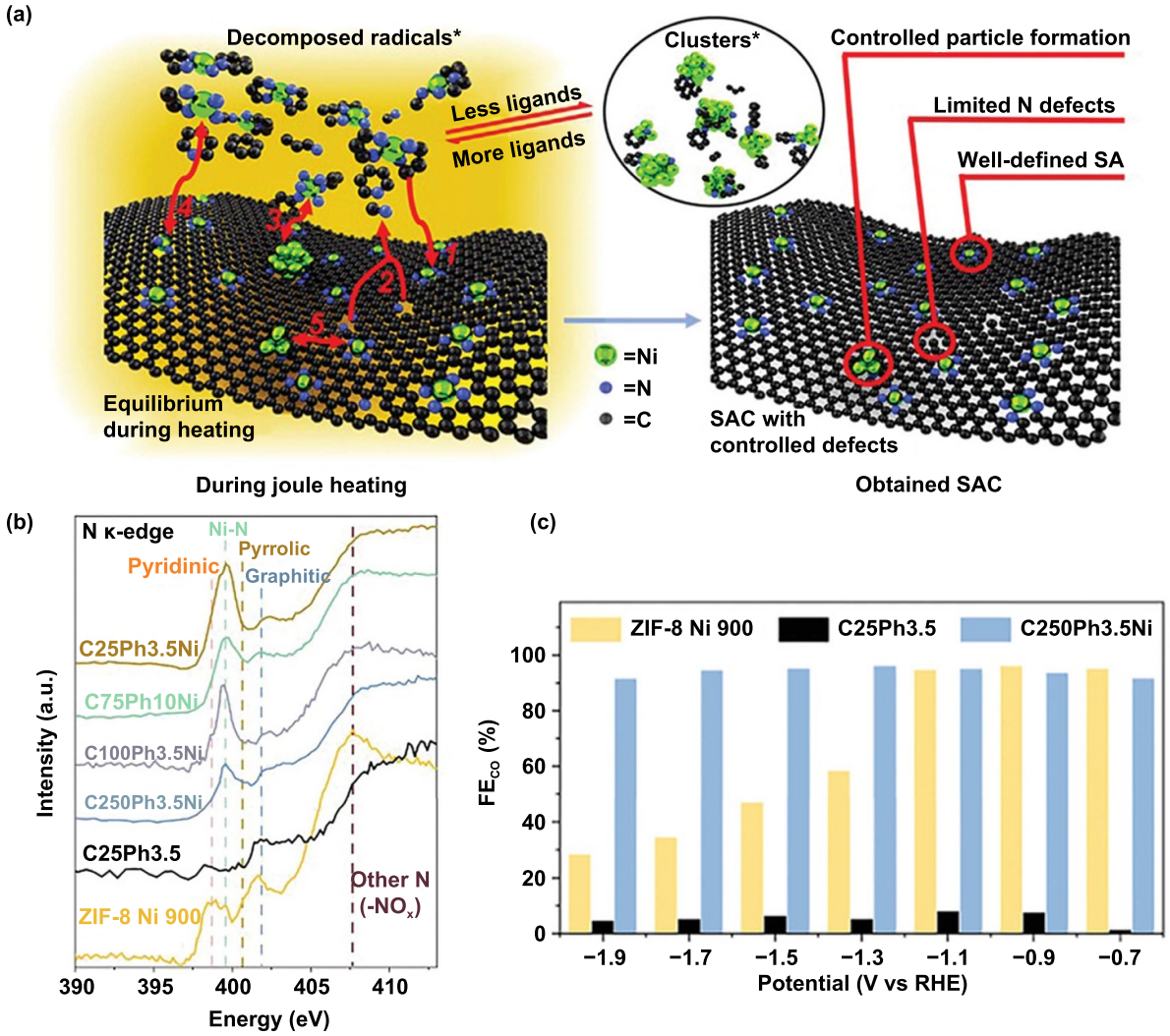

Figure 5. (a) Schematic illustration of the mechanism of the Joule heating processes for the production of Ni SACs. (b) N K-edge XAS spectra for $C_{\alpha}Ph_{\beta}Ni_{\gamma}$ (α, β, γ corresponds to their molar ratio of precursors) and ZIF-8 Ni 900. (c) Faradaic efficiency for CO production of ZIF-8 Ni 900, C25Ph3.5 and C250Ph3.5Ni. [55] John Wiley & Sons. © 2021 Wiley-VCH GmbH.

the porous graphene-based film (CoNG-JH). As illustrated in figure 6(b), the unique macropores and nanopores of the CoNG-JH monolithic electrode can effectively enhance mass transport and expose more active sites. HAADF-STEM image in figure 6(c) suggested the uniform dispersion of Co atoms on the support. As a result, the CoNG-JH electrode exhibited excellent catalytic activity compared with the state-of-the-art Co-based SACs and high stability toward the hydrogen evolution reaction (HER), as shown in figure 6(d).

As can be seen from the above reports, the Joule heating strategy has been widely used in the preparation of SACs in recent years. The strategy not only enables the transformation of nanoparticles into stably dispersed individual atoms by repeatedly turning on/off the Joule heating shockwaves, but also enables the regulation of the electronic structure by controlling nitrogen species, structural symmetry, etc. It can be expected that the Joule heating strategy is a very promising method for the scalable and controllable preparation of SACs.

3. Microwave heating

Microwave heating has similar advantageous features to Joule heating in that it is ultrafast, cost-effective and energy-saving, and has been considered as an effective heating strategy for preparing different types of nanomaterials in recent years [44, 50, 74–76]. The mechanisms of microwave heating synthesis can be mainly classified into two types. The first mechanism involves the rapid rotating of dipoles (e.g. OH groups) of polar materials (e.g. reduced graphene oxide (rGO)) in the presence of an oscillating electric field (>2000 million times per second), creating frictional heating. Secondly, for materials with charged particles (e.g. π electrons in graphene), microwave energy is dissipated as heat through eddy current losses due to the Maxwell Wagner effect [24]. Based on these two mechanisms, to achieve efficient microwave heating, three main requirements should be fulfilled: (a) abundant surface functional groups to provide enough frictional heat caused by rotation in an oscillating electric field; (b) sufficient electrical

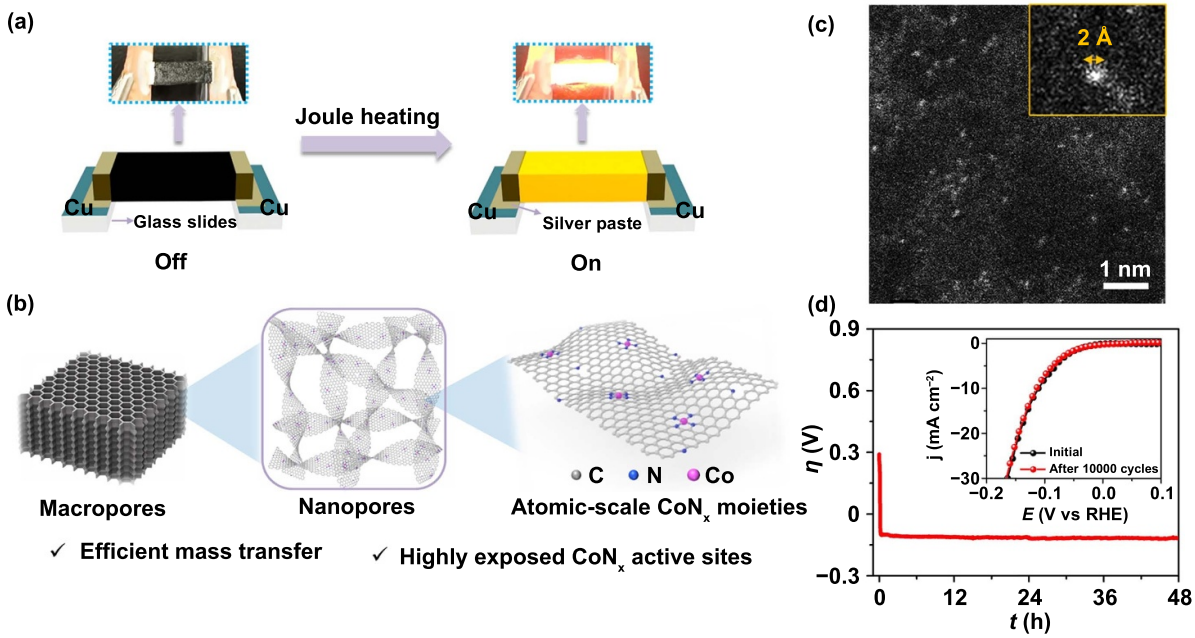

Figure 6. (a) Schematic of the preparation route of the self-supported CoNG-JH by Joule heating process. (b) The advantageous features of the CoNG-JH electrode. (c) HAADF-STEM image of CoNG-JH. The inset shows a single Co atom with the size of ∼2 Å. (d) Stability of CoNG-JH evaluated by the galvanostatic technique. The inset curve shows the LSV curves of CoNG-JH before and after cycling in 0.5 M H_2SO_4. Reproduced from [56], with permission from Springer Nature.

conductivity to generate eddy currents in the presence of microwaves; (c) high thermal conductivity for rapid and uniform diffusion of heat throughout the sample. In this regard, rGO with abundant functional groups and moderate conductivity can be used as an ideal microwave absorber. Specifically, the oxygen-rich functional groups in rGO rapidly absorb the microwaves to generate heat, leading to a sharp increase in temperature. At high temperature, the surface functional groups of rGO are quickly removed and the π-conjugation system is almost completely restored. This rapidly weakens the microwave absorption efficiency, thereby inducing fast self-quenching process [24]. As a result, rGO has been widely applied as microwave absorber and substrate for the synthesis of nanoparticles and SACs [44, 50, 76–86].

Fei and colleagues reported for the first time an ultrafast, efficient and universal microwave heating strategy to prepare a series of metal atoms (e.g. Co, Ni, Cu) supported on nitrogen-doped graphene [50]. The main synthetic procedure of the microwave heating method was illustrated in figure 7(a). In short, small amounts of Co precursors were added into AGO solution, during when the oxygen functional groups and amino groups in AGO could interact strongly with the Co ions. Then, the freeze-dried cobalt-containing AGO was processed in a 1000 W household microwave oven for 2 s under an Ar atmosphere to acquire the final product of Co–NG–MW. As shown in figure 7(b), Co-NG-MW exhibits an obvious symmetrical 2D band and a weaker D band, reflecting that the graphene structure was restored after the MW irradiation. As shown in figure 7(c), the x-ray diffraction pattern indicated that the interlayer distance of graphene was shortened from 0.78 nm ($2\theta = 11.3°$) to 0.34 nm ($2\theta = 26.5°$) in Co-NG-MW due to the removal of the surface functional groups in the graphene sheets. The atomic dispersion of Co in substrates was evidenced by the Fourier transform and wavelet transform of the Co *k*-edge EXAFS (figure 7(d)). By simply altering the metal precursors during the mixing step, this microwave heating strategy can be extended to synthesize other types of graphene-supported SACs (figure 7(e)). The resulting Co–NG–MW exhibited superior activity and cyclic stability in the HER (over 1000 cycles), which can be attributed to the strong coordination between the Co atoms and the adjacent C/N/O atoms induced by HT thermal shock.

In a followed study, Fei and colleagues found that the microwave heating strategy was able to generate SACs with differed composition and coordination configuration compared to those prepared by conventional prolonged pyrolysis method, thus leading to varied catalytic properties [44]. The Co–N–C catalyst obtained from microwave heating possesses a low-coordinated Co–N_2 moiety and high content of epoxide functional groups (denoted as Co–N_2–C/HO). However, another Co–N–C catalyst (denoted as Co–N_4–C/LO) with the Co–N_4 moiety and low content of epoxide groups was obtained by traditional prolonged annealing method (figure 8(a)). The high-resolution x-ray photoelectron spectroscopy (XPS) O 1s spectra were illustrated in figures 8(b) and (c), indicating that the oxygen content of Co–N_2–C/HO (7.9 at%) is significantly higher than that of Co–N_4–C/LO (5.70 at%) and that Co–N_2–C/HO contains abundant epoxy functional groups. The as-observed difference in composition and atomistic structure can be attributed to the much shorter processing time at the high temperature environment during the microwave synthesis of Co–N_2–C/HO. As a result of the synergistic effect of low coordination and epoxy functional group, Co–N_2–C/HO exhibited significantly improved

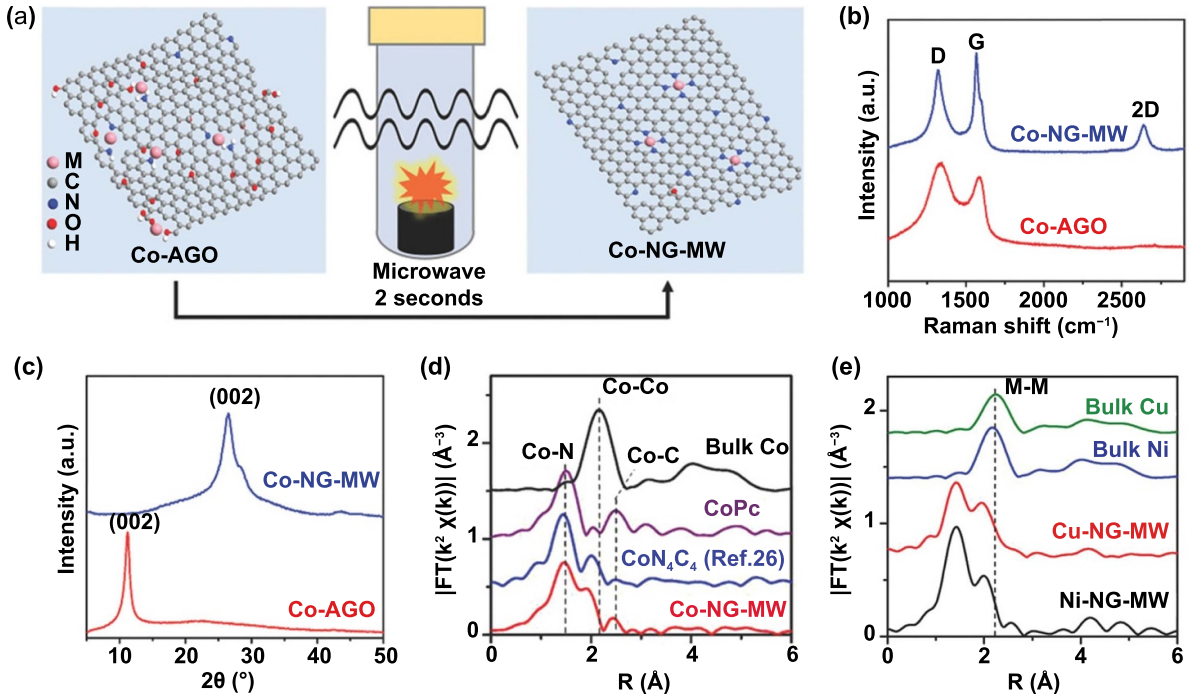

Figure 7. (a) Schematic of synthesis route of Co–NG–MW by microwave heating. (b) Raman spectra and (c) XRD patterns for Co-NG-MW and Co-AGO. (d) Fourier transforms of k^2-weighted Co K-edge EXAFS experimental data for Co–NG–MW and reference samples. (e) Fourier transform magnitudes of the K-edge EXAFS profiles (without phase correction) for Ni–NG–MW and Cu–NG–MW along with bulk metals. [50] John Wiley & Sons. © 2018 WILEY-VCH Verlag GmbH & Co. KGaA, Weinheim.

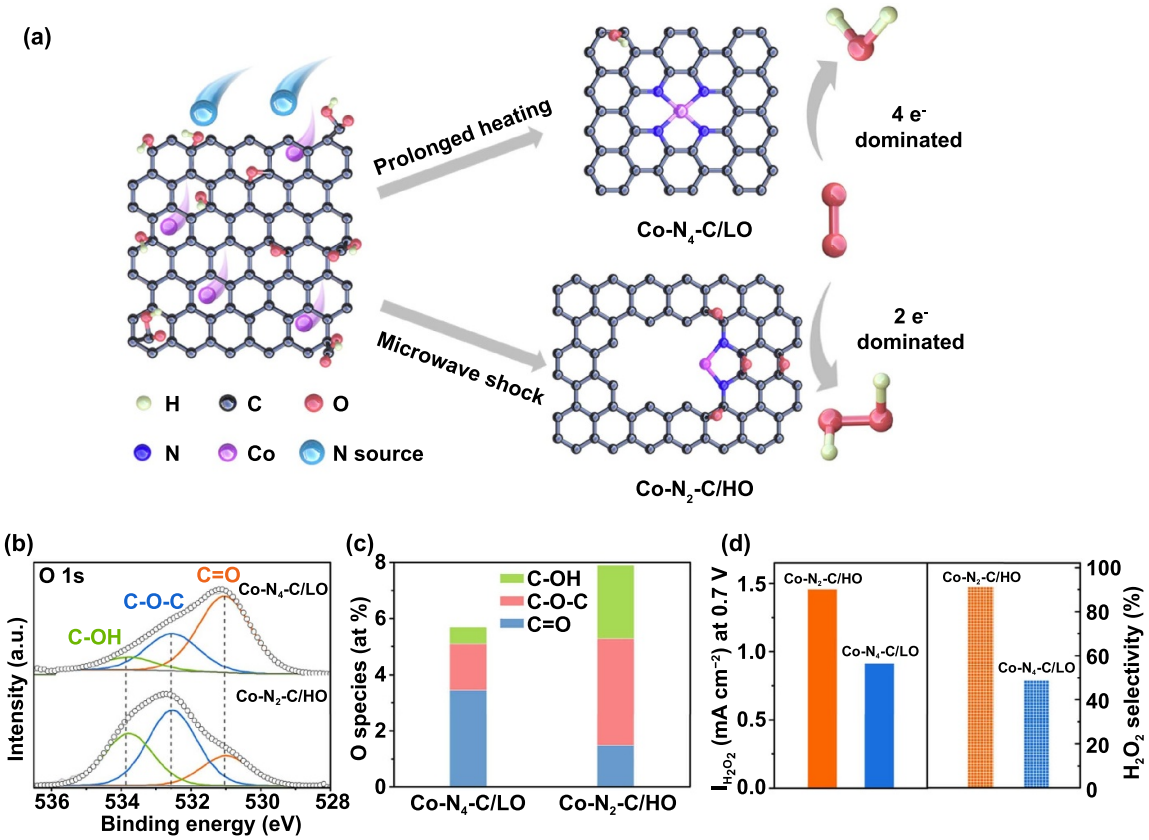

Figure 8. (a) Schematic diagram of the synthesis route of Co–N_4–C/LO and Co–N_2–C/HO by microwave shock and prolong heating. (b) High-resolution O 1s XPS spectra and (c) atomic percentages of oxygen species for Co–N_4–C/LO and Co–N_2–C/HO. (d) Comparison of the H_2O_2 current and H_2O_2 selectivity during the two-electron oxygen reduction reaction on Co–N_2–C/HO and Co–N_4–C/LO at 0.7 V. [44] John Wiley & Sons. © 2021 Wiley-VCH GmbH.

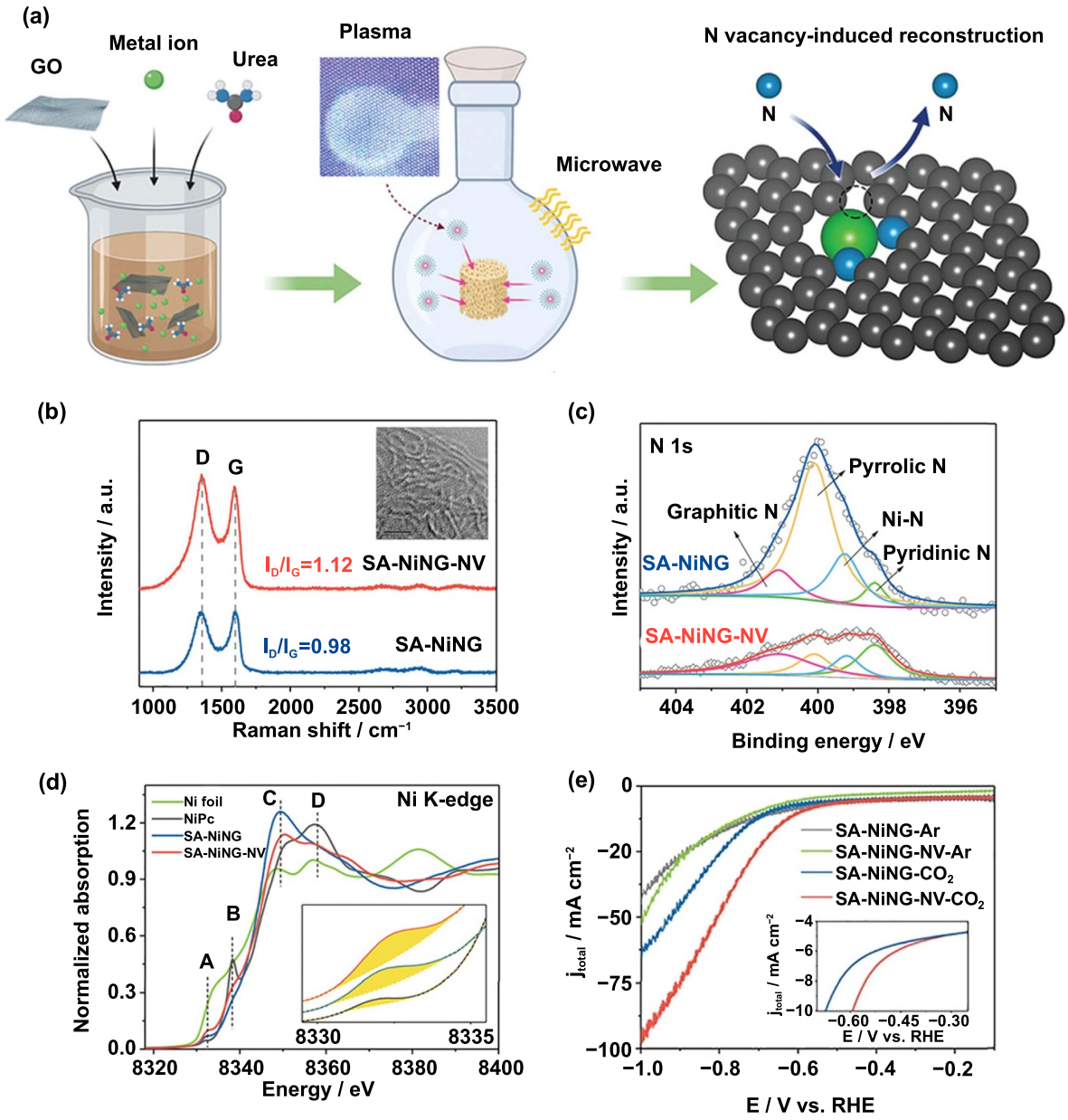

Figure 9. (a) Schematic illustration regarding the formation of SA-NiNG-NV by microwave treatment. (b) Raman spectra and (c) High-resolution N 1s XPS spectra for SA-NiNG and SA-NiNG-NV. (d) Ni K-edge XANES spectra of SA-NiNG-NV and SA-NiNG, Ni foil and NiPc. The inset in (d) shows the enlarged view of peak A. (e) LSV curves of SA-NiNG and SA-NiNG-NV in CO_2- and Ar-saturated 0.5 M $KHCO_3$. The inset shows the LSV polarization curves in low potential range. [46] John Wiley & Sons. © 2021 Wiley-VCH GmbH.

catalytic performance towards the two-electron oxygen reduction reaction for producing H_2O_2, such as large kinetic current density (11.3 mA cm^{-2} at 0.65 V), prominent selectivity (91.3%) and excellent mass activity (44.4 A g^{-1} at 0.65 V) (figure 8(d)), making it one of the best SACs for the electrosynthesis of H_2O_2.

In addition to the adjustment of the oxygen content, microwave heating has been utilized to realize the regulation of nitrogen species in SACs. Jia and colleagues adopted a low-pressure environment and longer microwave processing time to realize the conversion of pyrrolic N-defects neighbouring Ni sites to stable pyridinic N dominant Ni–N_2 coordination configuration by nitrogen vacancy-induced coordinative reconstruction strategy (figure 9(a)) [46]. To demonstrate the influence of microwave heating on the composition and structure of SACs, two samples with different microwave treatment times (i.e. SA-NiNG (5 s) and SA-NiNG-NV (60 s)) were prepared. The Raman spectra of the two above samples were presented in figure 9(b), where the intensity ratio of the D band to the G band (I_D/I_G) of SA-NiNG-NV is higher than that of SA-NiNG, suggesting the presence of more defects in SA-NiNG-NV. The high-resolution XPS N 1s spectra were illustrated in figure 9(c), indicating that the pyrrolic nitrogen was gradually converted

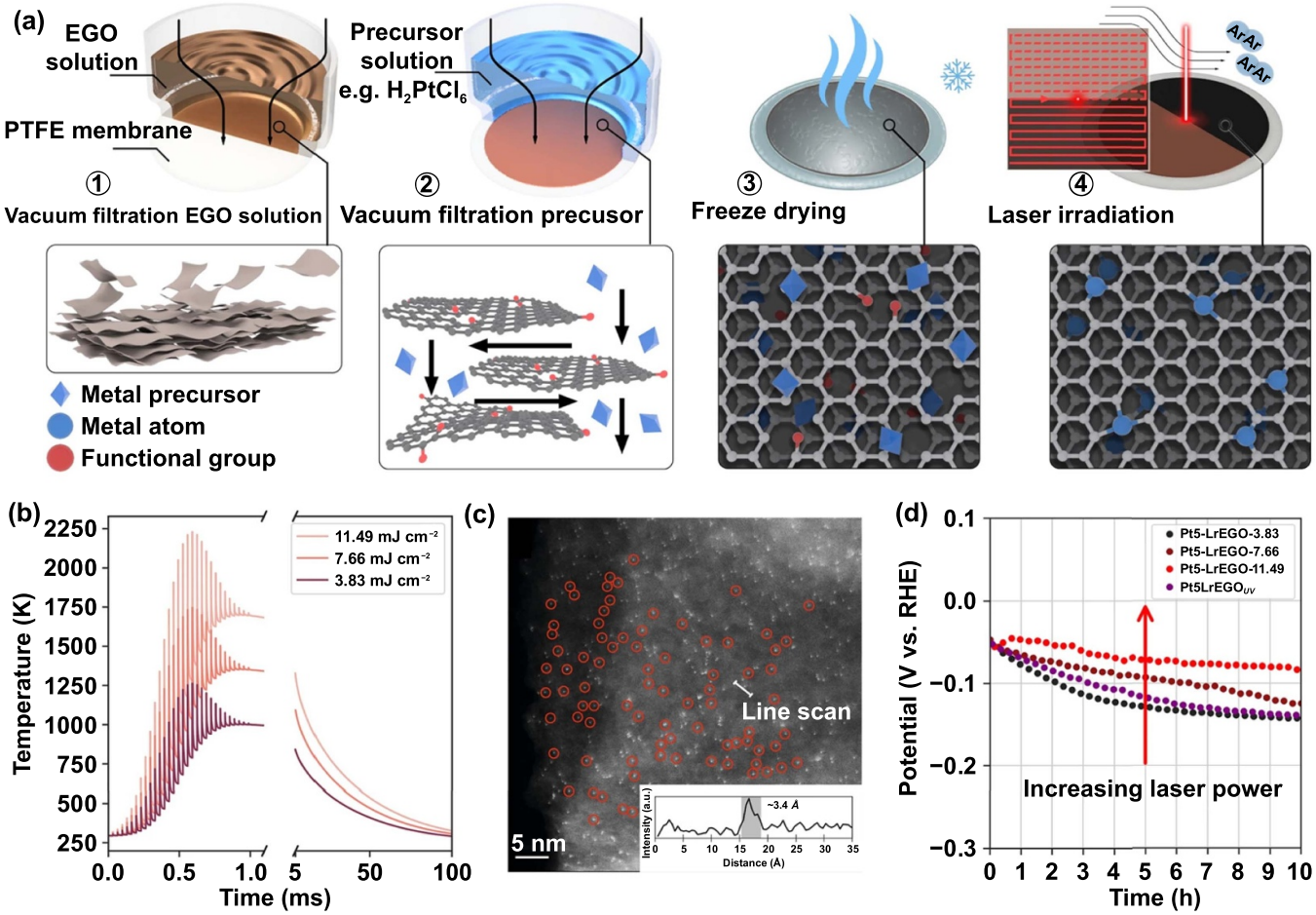

Figure 10. (a) Schematic illustration of the synthesis route of Pt-LrEGO by solid-state laser heating method. (b) The temperature of EGO films treated at various laser fluences with 1064 nm laser were modeled by COMSOL. (c) HAADF-STEM image of Pt-LrEGO. The inset shows the representative HAADF intensity profile. (d) Chronoamperometric response of Pt-LrEGO samples obtained at various laser fluences. Reproduced from [28]. CC BY 4.0.

to pyridinic nitrogen after a longer period of microwave treatment. Meanwhile, compared with the saturated Ni–N_4 structure of Ni phthalocyanine, the x-ray absorption near edge structure spectra of SA-NiNG-NV has a different rising edge intensity and structure, indicating that the catalyst has different symmetry around the Ni site (figure 9(d)). Combined with the above structure characterization, it is found that as the microwave process continues, the pyrrolic N atoms can be further removed and create vacancies, resulting in unstable pentagonal defects that could locally reconstruct into more stable pyridinic N dominant Ni–N species. Electrochemical measurements show that SA-NiNG-NV exhibited greatly improved activity and stability towards the CO_2RR, as shown in figure 9(e).

Based on the above discussion, the microwave heating method is general in preparing different types of SACs and it can lead to the formation of SACs with unconventional composition and structure, which can further result in enhanced catalytic properties. At the same time, compared with conventional methods, the microwave heating method has the following advantages: ultrafast heating/quenching rate, ultrahigh heating temperature, uniform temperature distribution throughout the substrates, suitability for carbon substrates with various dimensions, and low equipment requirements. With these advantages, the microwave heating synthesis is promised to realize the large-scale production and manufacturing of SACs through, for example, the integration with the roll-to-roll process like Joule heating [26, 74].

4. Other methods

After realizing the advantages of the thermal shock preparation for SACs, many researchers are devoted to the development of new heating strategies toward the rapid preparation of SACs [28, 51, 54, 57]. In addition to the Joule heating and microwave heating methods discussed above, the rapid heating preparation methods expand to solid-phase laser irradiation [28], flame-assisted method [57], arc-discharge method [51], etc.

Among them, solid-phase laser irradiation is fast, potentially scalable, and versatile for the large-scale production of SACs. Peng and colleagues reported for the first time a laser-induced solid-phase strategy to prepare SACs [28].

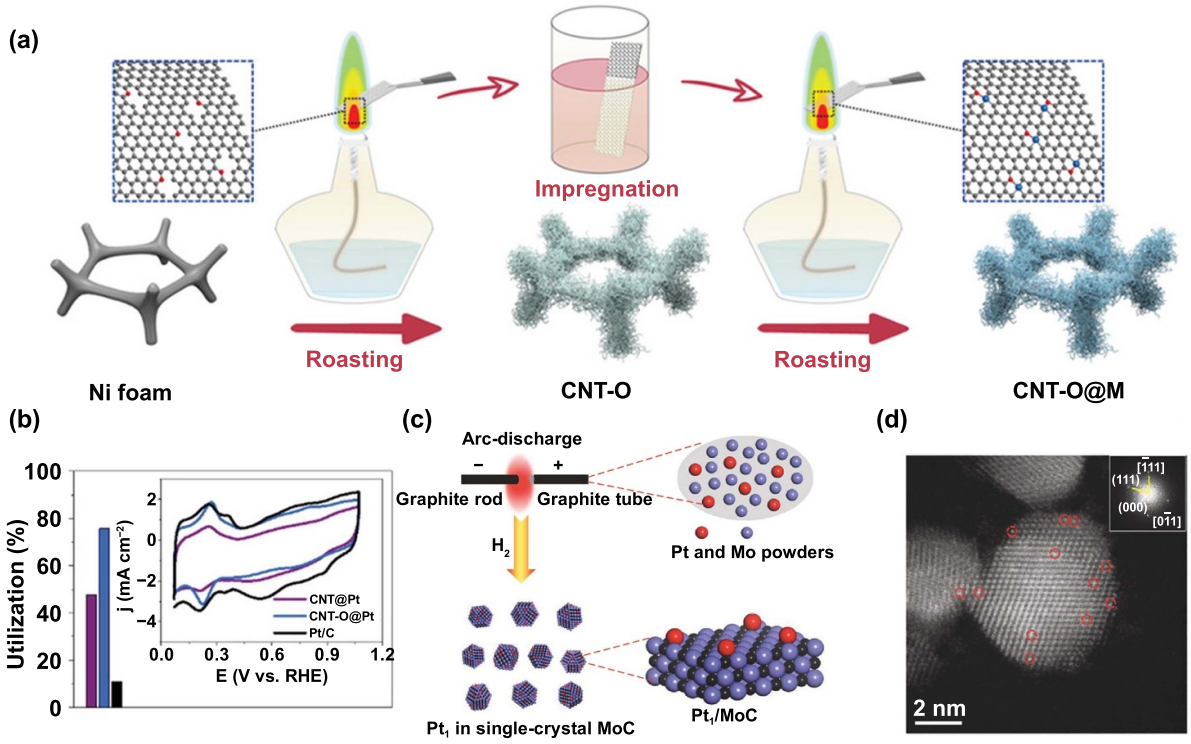

Figure 11. (a) Schematic for the synthesis route of CNT-O@M. (b) Active site utilization of CNT-O@Pt, CNT@P and Pt/C. The insets show CV curves of CNT-O@Pt, CNT@P and Pt/C [57]. John Wiley & Sons. Copyright © (2018) WILEY-VCH Verlag GmbH & Co. KGaA, Weinheim. (c) Schematic for the synthesis of Pt_1/MoC catalyst via arc-discharge strategy. (d) HAADF-STEM image of Pt_1/MoC. Reproduced from [51]. CC BY 4.0.

The schematic of the preparation process was shown in figure 10(a). First, the electrochemically prepared graphene oxide (EGO) films were prepared by vacuum filtration, and 1 ml of chloroplatinic acid (H_2PtCl_6) solution was filtered through the EGO films to acquire the Pt-EGO hydrogel films, which were immediately freeze-dried. Then, the Pt-EGO films were scanned quickly by laser in an Ar atmosphere to prepare Pt SACs (Pt-LrEGO). To uncover the synthesis mechanism, the influences of different laser types and fluences were studied. It was found that the mechanism is based on the simultaneous photoreduction of graphene oxide and metal precursors. In this process, the absorbed laser energy was quickly transformed into local heat through the photothermal effect, increasing the local temperature. Figure 10(b) shows that the ultrafast heating of about 1 ms reached up to 1692.2 K, and the temperature was quickly reduced to 298.15 K in about 108 ms through the simulation temporal thermal profile. Figure 10(b) also shows the simulated temperature of different intensity lasers. The HAADF-STEM image exhibits the uniform dispersion of Pt atoms on the LrEGO support existing as bright dots with a diameter of ∼0.34 nm, corresponding to an individual Pt atom, as shown as figure 10(c). Electrochemical measurements towards the HER suggest that the catalysts prepared with different laser powers exhibited similar activity but the stability increased with laser powers (figure (d)), which can be ascribed to the fact that the fast heating and quenching during the laser processing prevent the aggregation and diffusion of the individual atoms, and the brief HT shockwaves may be beneficial to the formation of a more stable bond between the graphene support and the single atoms.

In another work, Li and colleagues developed a simple flame-assisted strategy to prepare well-defined O-coordinated SACs on integrated carbon nanotube arrays (CNT-O@M) [57]. In this preparation process, oxygen doped carbon nanotubes (CNT-O) were constructed on Ni substrate via flame-assisted method [87–90]. The carbon source for the formation of carbon nanotubes was derived from the large numbers of carbonaceous molecules released by the inner flame of the alcohol lamp during the roasting process. Then, the single atoms were confined to CNT-O through strong coordination with the oxygen functional groups during the second flame-assisted treatment progress (figure 11(a)). By adopting such flame-assisted processes, CNT-O@Co and CNT-O@Pt were successfully synthesized. As shown in figure 11(b), the active site utilization of CNT-O@Pt is as high as 75.7%.

In addition, arc discharge treatment has been used to achieve ultrahigh temperature thermal shock for the synthesis of SACs. Bi and colleagues successfully developed a facile and controllable ultrahigh temperature (up to 4000 °C) via a one-step arc-discharge treatment to synthesize Pt SACs (figure 11(c)) [51]. The high temperature provided the

Table 1. Summary of key characteristics of various ultrafast heating strategies for the synthesis of SACs.

Preparation methods	Principles	Advantages	Disadvantages	Time consumption	Mass loading	Yield	Reference
Microwave heating	Dipolar polarization and ionic conduction	Simple equipment, different atmospheres, non-contact	Special substrates	A few seconds	0.1–2.1 wt%	Low	[44–46, 50]
Joule heating	Joule's law	Controllable condition, scalable	Easily contaminated by sample stage	Hundreds of milliseconds	0.2–3.0 wt%	High	[26, 52, 56]
Laser irradiation	Photo-thermo-chemical reaction	Versatile, non-thermal radiation	Special equipment	A few seconds	0.4 wt%	High	[28]
Flame-assisted method	Gas phase self-assembly	Simple equipment, ambient atmosphere	Uncontrollable	Tens of seconds	2.1 wt%	Low	[57]
Arc-discharge method	Arc discharge	Controllable, ultrahigh temperature (up to 4000 °C)	Complex equipment	A few minutes	2.0 wt%	Low	[51]

sufficient activation energy for atom dispersion and overall stability by formation of strong Pt–MoC interactions. As shown in figure 11(d), HAADF-STEM images clearly suggest that Pt atoms are dispersed as single atoms. At the same time, HT-stabilized Pt_1/MoC exhibited excellent catalytic performance and outstanding thermal stability for selective quinoline hydrogenation.

5. Conclusion

In conclusion, we have summarized various ultrafast heating strategies for the synthesis of SACs. The key characteristics such as the working principles, advantages, disadvantages and time consumption for each method are summarized in table 1. These strategies can prepare SACs in one simple step under extreme heating conditions (ultrahigh temperature and ultrafast heating/quenching rate), which can avoid uncontrollable factors that are common in conventional multi-step procedures and greatly shorten the preparation time. Benefiting from the extreme conditions of ultrafast heating synthesis, it has many advantages compared with conventional methods. Firstly, ultrafast synthesis strategies have the characteristics of fast ignition, rapid heating and instant quenching, which hinders the migration and aggregation of single atoms, making it possible for high metal loading in SACs. At the same time, it can generate ultrahigh temperature instantaneously that is critical for single-atom stabilization as it provides the sufficient activation energy to facilitate the formation of bonds between single atoms and the substrate, resulting in excellent thermal and chemical stability during synthesis and catalytic operation. Secondly, the uniformity of the product can be guaranteed by using ultrafast synthesis strategies due to the facts that (a) before the ultrafast heating process, the precursors were typically treated with liquid-phase mixing, which could ensure the even mixing between the metal and substrate precursors, (b) the ultrafast heating strategies such as microwave heating and Joule heating can generate uniform heat distribution throughout the whole material, and (c) the high thermal conductivity of substrates, such as nanocarbons or metals, allows for rapid and uniform heat dispersion throughout the sample. Last but not least, the ultrafast heating strategies typically require no sophisticated and complicated instrumentations, along with high energy and time efficiency, thus having the potential to produce SACs in a scalable manner when combined with the roll-to-roll system [26, 91], continuous fly-through [92] or microfluidic technology [93].

However, these ultrafast heating strategies for synthesizing SACs still have some limitations and challenges. Firstly, all ultrafast heating strategies face challenges in precise measurement and control in reacting temperature. At present, a thermocouple is typically used for temperature measurement. However, due to the facts that the thermocouples can also be heated by microwave, Joule heating and other methods, and that the existence of spacing between the thermocouple and the sample will cause excessive temperature attenuation, it is difficult to directly measure the temperature during the ultrafast heating process. Another common method is to employ blackbody radiation theory to evaluate the temperature through fitting the spectrum with the blackbody radiation equation. However, this process involves some expensive equipment and software, and there is still a large relative deviation in the evaluation of temperature. Therefore, the precise measurement of the sample temperature during the ultrafast synthesis process remains a big challenge.

Secondly, increasing the metal loading and the atom utilization efficiency is critical to the development of high-performance SACs. At present, the metal loading in SACs is generally kept low enough to avoid aggregation during synthesis and catalytic operation, which limits the number of active sites and thus catalytic activity. Although ultrafast heating strategies are expected to be beneficial in increasing the metal loading as it can reverse the OR process and prevent the aggregation and diffusion of the individual atoms since they can minimize the exposure of metal atoms at high-energy environment. Unfortunately, this perceived advantage has not been realized probably due to the harsh reactive conditions imposed on the sample by the ultrahigh temperature. In order to further increase the metal loading, it would be desirable to finely control and monitor the reactive temperature to avoid overheating. Meanwhile, introducing nanoporosity and creating abundant coordinating or defective sites in the substrates could potentially provide additional anchoring sites for loading more metal sites and enhance the exposure of reactive interfaces toward improved atom utilization efficiency.

Thirdly, it remains a challenge to establish a correlation between the synthetic conditions or parameters during the ultrafast heating process and the structure of the obtained SACs, which precludes the rational and controllable synthesis and design of SACs. Despite the considerably high performance exhibited by the SACs prepared by ultrafast heating methods, the exploration of SACs toward specific catalytic processes and the optimization in performance are mainly conducted via a trial-and-error manner without much guidance. To partially solve this problem, it is critical to finely tune the synthetic conditions and parameters during the ultrafast heating synthesis and systematically study their effects on the composition, structure, and morphology of SACs. Additionally, it would be helpful to perform studies on the structural evolution and formation mechanism of SACs by, for example, *in situ* monitoring and characterizing the reacting intermediates generated or released during the ultrafast heating synthesis.

In short, despite the many challenges ahead, the ultrafast heating strategies for synthesizing SACs will continue to receive extensive attention and applications in the synthesis of SACs as well as other types of nanomaterials such as high-entropy alloys and will open up a new avenue for the cost-effective and scalable production of high-performance catalysts for various catalytic processes.

Acknowledgments

H F acknowledges financial support from the National Natural Science Foundation of China (Grant No. 51902099), Hunan high-level talent gathering project (Grant No. 2019RS1021), Fundamental Research Funds for the Central Universities (Grant No. 531119200087), and the Innovative Research Groups of Hunan Province (Grant No. 2020JJ1001).

ORCID iD

Huilong Fei https://orcid.org/0000-0002-4216-5810

References

[1] Lang R, Du X R, Huang Y K, Jiang X Z, Zhang Q, Guo Y L, Liu K P, Qiao B T, Wang A Q and Zhang T 2020 Single-atom catalysts based on the metal-oxide interaction *Chem. Rev.* **120** 11986–2043

[2] Fei H L, Dong J C, Chen D L, Hu T D, Duan X D, Shakir I, Huang Y and Duan X F 2019 Single atom electrocatalysts supported on graphene or graphene-like carbons *Chem. Soc. Rev.* **48** 5207–41

[3] Yang X F, Wang A Q, Qiao B T, Li J, Liu J Y and Zhang T 2013 Single-atom catalysts: a new frontier in heterogeneous catalysis *Acc. Chem. Res.* **46** 1740–8

[4] Li Z J, Wang D H, Wu Y E and Li Y D 2018 Recent advances in the precise control of isolated single-site catalysts by chemical methods *Natl Sci. Rev.* **5** 673–89

[5] Fu Q, Saltsburg H and Flytzani-Stephanopoulos M 2003 Active nonmetallic Au and Pt species on ceria-based water-gas shift catalysts *Science* **301** 935–8

[6] Hackett S F J, Brydson R M, Gass M H, Harvey I, Newman A D, Wilson K and Lee A F 2007 High-activity, single-site mesoporous Pd/Al_2O_3 catalysts for selective aerobic oxidation of allylic alcohols *Angew. Chem., Int. Ed.* **46** 8593–6

[7] Qiao B T, Wang A Q, Yang X F, Allard L F, Jiang Z, Cui Y T, Liu J Y, Li J and Zhang T 2011 Single-atom catalysis of CO oxidation using Pt_1/FeO_x *Nat. Chem.* **3** 634–41

[8] Peng Y, Lu B Z and Chen S W 2018 Carbon-supported single atom catalysts for electrochemical energy conversion and storage *Adv. Mater.* **30** 1801995

[9] Xi J B, Jung H S, Xu Y, Xiao F, Bae J W and Wang S 2021 Synthesis strategies, catalytic applications, and performance regulation of single-atom catalysts *Adv. Funct. Mater.* **31** 2008318

[10] Liu J Y 2017 Catalysis by supported single metal atoms *ACS Catal.* **7** 34–59

[11] Shi Y S, Zhao C Y, Wei H S, Guo J H, Liang S X, Wang A Q, Zhang T, Liu J Y and Ma T L 2014 Single-atom catalysis in mesoporous photovoltaics: the principle of utility maximization *Adv. Mater.* **26** 8147–53

[12] Zhang W and Zheng W T 2016 Single atom excels as the smallest functional material *Adv. Funct. Mater.* **26** 2988–93

[13] Mitchell S, Vorobyeva E and Pérez-Ramírez J 2018 The multifaceted reactivity of single-atom heterogeneous catalysts *Angew. Chem., Int. Ed.* **57** 15316–29

[14] Zhu C Z, Fu S F, Shi Q R, Du D and Lin Y H 2017 Single-atom electrocatalysts *Angew. Chem., Int. Ed.* **56** 13944–60

[15] Li X Y, Rong H P, Zhang J T, Wang D S and Li Y D 2020 Modulating the local coordination environment of single-atom catalysts for enhanced catalytic performance *Nano Res.* **13** 1842–55

[16] Wang J, Li Z J, Wu Y E and Li Y D 2018 Fabrication of single-atom catalysts with precise structure and high metal loading *Adv. Mater.* **30** 1801649

[17] Liu J J *et al* 2021 Edge-hosted $Fe–N_3$ sites on a multiscale porous carbon framework combining high intrinsic activity with efficient mass transport for oxygen reduction *Chem. Catal.* **1** 1291–307

[18] Liu J J, Gong Z C, Yan M M, He G C, Gong H S, Ye G L and Fei H L 2022 Electronic structure regulation of single-atom catalysts for electrochemical oxygen reduction to H_2O_2 *Small* **18** 2103824

[19] Zhang B, Zheng Y J, Ma T, Yang C D, Peng Y F, Zhou Z H, Zhou M, Li S, Wang Y H and Cheng C 2021 Designing MOF nanoarchitectures for electrochemical water splitting *Adv. Mater.* **33** 2006042

[20] Xiong H F, Datye A K and Wang Y 2021 Thermally stable single-atom heterogeneous catalysts *Adv. Mater.* **33** 2004319

[21] Qiao B T, Liang J X, Wang A Q, Xu C Q, Li J, Zhang T and Liu J Y 2015 Ultrastable single-atom gold catalysts with strong covalent metal-support interaction (CMSI) *Nano Res.* **8** 2913–24

[22] Hansen T W, DeLaRiva A T, Challa S R and Datye A K 2013 Sintering of catalytic nanoparticles: particle migration or Ostwald ripening? *Acc. Chem. Res.* **46** 1720–30

[23] Ouyang R H, Liu J X and Li W X 2013 Atomistic theory of Ostwald ripening and disintegration of supported metal particles under reaction conditions *J. Am. Chem. Soc.* **135** 1760–71

[24] Wan C Z and Duan X F 2019 Microwave shock synthesis beyond thermodynamic equilibrium *Matter* **1** 555–7

[25] Giugni A 2019 Non-locality by nanoconfinement *Nat. Nanotechnol.* **14** 814–5

[26] Yao Y G *et al* 2019 High temperature shockwave stabilized single atoms *Nat. Nanotechnol.* **14** 851–7

[27] Du C F, Sun X L, Yu H, Fang W, Jing Y, Wang Y H, Li S Q, Liu X H and Yan Q Y 2020 $V_4C_3T_x$ MXene: a promising active substrate for reactive surface modification and the enhanced electrocatalytic oxygen evolution activity *InfoMat* **2** 950–9

[28] Peng Y D, Cao J Y, Sha Y, Yang W J, Li L and Liu Z 2021 Laser solid-phase synthesis of single-atom catalysts *Light Sci. Appl.* **10** 168

[29] O'Neill B J, Jackson D H K, Lee J, Canlas C, Stair P C, Marshall C L, Elam J W, Kuech T F, Dumesic J A and Huber G W 2015 Catalyst design with atomic layer deposition *ACS Catal.* **5** 1804–25

[30] Cheng N C and Sun X L 2017 Single atom catalyst by atomic layer deposition technique *Chin. J. Catal.* **38** 1508–14

[31] Chen Y X, Huang Z W, Ma Z, Chen J M and Tang X F 2017 Fabrication, characterization, and stability of supported single-atom catalysts *Catal. Sci. Technol.* **7** 4250–8

[32] Zhang L Z *et al* 2018 Graphene defects trap atomic Ni species for hydrogen and oxygen evolution reactions *Chem* **4** 285–97

[33] Long Y P *et al* 2021 Hedgehog artificial macrophage with atomic-catalytic centers to combat drug-resistant bacteria *Nat. Commun.* **12** 6143

[34] Gao Y *et al* 2021 Activity trends and mechanisms in peroxymonosulfate-assisted catalytic production of singlet oxygen over atomic metal-N-C catalysts *Angew. Chem., Int. Ed.* **60** 22513–21

[35] Li S, Chen B B, Wang Y, Ye M Y, van Aken P A, Cheng C and Thomas A 2021 Oxygen-evolving catalytic atoms on metal carbides *Nat. Mater.* **20** 1240–7

[36] Liu L C, Meira D M, Arenal R, Concepcion P, Puga A V and Corma A 2019 Determination of the evolution of heterogeneous single metal atoms and nanoclusters under reaction conditions: which are the working catalytic sites? *ACS Catal.* **9** 10626–39

[37] Ji S F, Chen Y J, Wang X L, Zhang Z D, Wang D S and Li Y D 2020 Chemical synthesis of single atomic site catalysts *Chem. Rev.* **120** 11900–55

[38] Hu Y F, Li H X, Li Z S, Li B L, Wang S Y, Yao Y C and Yu C L 2021 Progress in batch preparation of single-atom catalysts and application in sustainable synthesis of fine chemicals *Green Chem.* **23** 8754–94

[39] Wang A Q, Li J and Zhang T 2018 Heterogeneous single-atom catalysis *Nat. Rev. Chem.* **2** 65–81

[40] Wang Y X *et al* 2020 Advanced electrocatalysts with single-metal-atom active sites *Chem. Rev.* **120** 12217–314

[41] Ma Y F, Chi B L, Liu W, Cao L N, Lin Y, Zhang X H, Ye X X, Wei S Q and Lu J L 2019 Tailoring of the proximity of platinum single atoms on CeO_2 using phosphorus boosts the hydrogenation activity *ACS Catal.* **9** 8404–12

[42] Qin R X, Liu K L, Wu Q Y and Zheng N F 2020 Surface coordination chemistry of atomically dispersed metal catalysts *Chem. Rev.* **120** 11810–99

[43] Yao Y G *et al* 2018 Carbothermal shock synthesis of high-entropy-alloy nanoparticles *Science* **359** 1489–94

[44] Gong H S *et al* 2022 Low-coordinated Co–N–C on oxygenated graphene for efficient electrocatalytic H_2O_2 production *Adv. Funct. Mater.* **32** 2106886

[45] Meng R W *et al* 2021 An oxygenophilic atomic dispersed Fe–N–C catalyst for lean-oxygen seawater batteries *Adv. Energy Mater.* **11** 2100683

[46] Jia C *et al* 2021 Nitrogen vacancy induced coordinative reconstruction of single-atom Ni catalyst for efficient electrochemical CO_2 reduction *Adv. Funct. Mater.* **31** 2107072

[47] Ye S H *et al* 2019 Highly stable single Pt atomic sites anchored on aniline-stacked graphene for hydrogen evolution reaction *Energy Environ. Sci.* **12** 1000–7

[48] Noh W Y, Kim E M, Kim K Y, Kim J H, Jeong H Y, Sharma P, Lee G, Jang J W, Joo S H and Lee J S 2020 Immobilizing single atom catalytic sites onto highly reduced carbon hosts: fe–N_4/CNT as a durable oxygen reduction catalyst for Na–air batteries *J. Mater. Chem.* A **8** 18891–902

[49] Li Q D *et al* 2020 Microwave-enabled incorporation of single atomic Cu catalytic sites in holey graphene: unifying structural requirements of a carbon matrix for simultaneous achievement of high activity and long-term durability *ACS Appl. Energy Mater.* **3** 8266–75

[50] Fei H L *et al* 2018 Microwave-assisted rapid synthesis of graphene-supported single atomic metals *Adv. Mater.* **30** 1802146

[51] Bi Q Y, Yuan X T, Lu Y, Wang D, Huang J, Si R, Sui M L and Huang F Q 2020 One-step high-temperature-synthesized single-atom platinum catalyst for efficient selective hydrogenation *Research* **2020** 9140841

[52] Jiang D *et al* 2021 Tailoring the local environment of platinum in single-atom Pt_1/CeO_2 catalysts for robust low-temperature CO oxidation *Angew. Chem., Int. Ed.* **60** 26054–62

[53] Lu Q, Wu H, Zheng X R, Chen Y N, Rogach A L, Han X P, Deng Y D and Hu W B 2021 Encapsulating cobalt nanoparticles in interconnected N-doped hollow carbon nanofibers with enriched Co–N–C moiety for enhanced oxygen electrocatalysis in Zn-air batteries *Adv. Sci.* **8** 2101438

[54] Du J Y, Wu G, Liang K, Yang J, Zhang Y D, Lin Y, Zheng X S, Yu Z Q, Wu Y E and Hong X 2021 Rapid controllable synthesis of atomically dispersed Co on carbon under high voltage within one minute *Small* **17** 2007264

[55] Xi D W *et al* 2021 Limiting the uncoordinated N species in M–N_x single-atom catalysts toward electrocatalytic CO_2 reduction in broad voltage range *Adv. Mater.* 2104090

[56] Xing L L, Liu R, Gong Z C, Liu J J, Liu J B, Gong H S, Huang K and Fei H L 2021 Ultrafast Joule heating synthesis of hierarchically porous graphene-based Co–N–C single-atom monoliths *Nano Res.* (https://doi.org/10.1007/s12274-021-4046-z)

[57] Li J Z, Li H, Xie W F, Li S J, Song Y K, Fan K, Lee J Y and Shao M F 2022 Flame-assisted synthesis of O-coordinated single-atom catalysts for efficient electrocatalytic oxygen reduction and hydrogen evolution reaction *Small Methods* **6** 2101324

[58] Wyss K M, Luong D X and Tour J M 2022 Large-scale syntheses of 2D materials: flash Joule heating and other methods *Adv. Mater.* **34** 2106970

[59] Yang C P, Yao Y G, He S M, Xie H, Hitz E and Hu L B 2017 Ultrafine silver nanoparticles for seeded lithium deposition toward stable lithium metal anode *Adv. Mater.* **29** 1702714

[60] Li Y J *et al* 2017 *In situ*, fast, high-temperature synthesis of nickel nanoparticles in reduced graphene oxide matrix *Adv. Energy Mater.* **7** 1601783

[61] Murakami R K and Villas-Boas V 1999 Nanocrystalline magnetic materials obtained by flash annealing *Mater. Res.* **2** 67–73

[62] Cologna M, Rashkova B and Raj R 2010 Flash sintering of nanograin zirconia in <5 s at 850 °C *J. Am. Ceram. Soc.* **93** 3556–9

[63] Fujita J I, Nakazawa S, Ichihashi T, Ishida M, Kaito T and Matsui S 2007 Graphitic tube transformation of FIB-CVD pillar by Joule heating with flash discharge *Microelectron. Eng.* **84** 1507–10

[64] Song X Z, Li N, Zhang H, Wang L, Yan Y J, Wang H, Wang L Y and Bian Z Y 2020 Graphene-supported single nickel atom catalyst for highly selective and efficient hydrogen peroxide production *ACS Appl. Mater. Interfaces* **12** 17519–27

[65] He X H *et al* 2020 Mechanochemical kilogram-scale synthesis of noble metal single-atom catalysts *Cell Rep. Phys. Sci.* **1** 100004

[66] Gao J J *et al* 2020 Enabling direct H_2O_2 production in acidic media through rational design of transition metal single atom catalyst *Chem* **6** 658–74

[67] Long G F, Wan K, Liu M Y, Liang Z X, Piao J H and Tsiakaras P 2017 Active sites and mechanism on nitrogen-doped carbon catalyst for hydrogen evolution reaction *J. Catal.* **348** 151–9

[68] Liu Y M, Yu H T, Quan X, Chen S, Zhao H M and Zhang Y B 2014 Efficient and durable hydrogen evolution electrocatalyst based on nonmetallic nitrogen doped hexagonal carbon *Sci. Rep.* **4** 6843

[69] Jin Q Y, Ren B W, Cui H and Wang C X 2021 Nitrogen and cobalt Co-doped carbon nanotube films as binder-free trifunctional electrode for flexible zinc-air battery and self-powered overall water splitting *Appl. Catal.* B **283** 119643

[70] Ma T Y, Dai S and Qiao S Z 2016 Self-supported electrocatalysts for advanced energy conversion processes *Mater. Today* **19** 265–73

[71] Liu R *et al* 2021 Design of aligned porous carbon films with single-atom Co–N–C sites for high-current-density hydrogen generation *Adv. Mater.* **33** 2103533

[72] Son H J, Kim M J and Ahn S H 2021 Monolithic Co–N–C membrane integrating Co atoms and clusters as a self-supporting multi-functional electrode for solid-state zinc-air batteries and self-powered water splitting *Chem. Eng. J.* **414** 128739

[73] Cai G R, Zhang W, Jiao L, Yu S H and Jiang H L 2017 Template-directed growth of well-aligned MOF arrays and derived self-supporting electrodes for water splitting *Chem* **2** 791–802

[74] Qiao H Y *et al* 2021 Scalable synthesis of high entropy alloy nanoparticles by microwave heating *ACS Nano* **15** 14928–37

[75] Xu S M *et al* 2019 Uniform, scalable, high-temperature microwave shock for nanoparticle synthesis through defect engineering *Matter* **1** 759–69

[76] Voiry D, Yang J, Kupferberg J, Fullon R, Lee C, Jeong H Y, Shin H S and Chhowalla M 2016 High-quality graphene via microwave reduction of solution-exfoliated graphene oxide *Science* **353** 1413–6

[77] Xu S M *et al* 2017 *Universal, in situ* transformation of bulky compounds into nanoscale catalysts by high-temperature pulse *Nano Lett.* **17** 5817–22

[78] Gong Z C *et al* 2021 Constructing a graphene-encapsulated amorphous/crystalline heterophase NiFe alloy by microwave thermal shock for boosting the oxygen evolution reaction *ACS Catal.* **11** 12284–92

[79] Liu R Z, Zhang Y, Ning Z J and Xu Y X 2017 A catalytic microwave process for superfast preparation of high-quality reduced graphene oxide *Angew. Chem., Int. Ed.* **56** 15677–82

[80] Liu Z, Zhang X Y, Poyraz S, Surwade S P and Manohar S K 2010 Oxidative template for conducting polymer nanoclips *J. Am. Chem. Soc.* **132** 13158–9

[81] Lin Y, Baggett D W, Kim J W, Siochi E J and Connell J W 2011 Instantaneous formation of metal and metal oxide nanoparticles on carbon nanotubes and graphene via solvent-free microwave heating *ACS Appl. Mater. Interfaces* **3** 1652–64

[82] Poyraz S, Zhang L, Schroder A and Zhang X Y 2015 Ultrafast microwave welding/reinforcing approach at the interface of thermoplastic materials *ACS Appl. Mater. Interfaces* **7** 22469–77

[83] Tian Y R, Yang X, Nautiyal A, Zheng Y Y, Guo Q P, Luo J J and Zhang X Y 2019 One-step microwave synthesis of MoS_2/MoO_3@graphite nanocomposite as an excellent electrode material for supercapacitors *Adv. Compos. Hybrid Mater.* **2** 151–61

[84] Liu Z *et al* 2011 Poptube approach for ultrafast carbon nanotube growth *Chem. Commun.* **47** 9912–4

[85] Zhang X Y and Manohar S K 2006 Microwave synthesis of nanocarbons from conducting polymers *Chem. Commun.* **23** 2477–9

[86] Bi Y H, Nautiyal A, Zhang H P, Luo J J and Zhang X Y 2018 One-pot microwave synthesis of NiO/MnO_2 composite as a high-performance electrode material for supercapacitors *Electrochim. Acta* **260** 952–8

[87] Liu K, Li Z H, Xie W F, Li J B, Rao D M, Shao M F, Zhang B S and Wei M 2018 Oxygen-rich carbon nanotube networks for enhanced lithium metal anode *Energy Storage Mater.* **15** 308–14

[88] Vander Wal R L, Ticich T M and Curtis V E 2000 Flame synthesis of metal-catalyzed single-wall carbon nanotubes *J. Phys. Chem.* A **104** 7209–17

[89] Xiong X H, Zhao P, Ren R, Cui X and Ji S D 2019 Flame-synthesis of carbon nanotube forests on metal mesh structure: dependence, morphology, and application *Nanomaterials* **9** 1188

[90] Han S, Yang J, Li X F, Li W, Zhang X T, Koratkar N and Yu Z Z 2020 Flame synthesis of superhydrophilic carbon nanotubes/Ni foam decorated with Fe_2O_3 nanoparticles for water purification via solar steam generation *ACS Appl. Mater. Interfaces* **12** 13229–38

[91] Liu Y J, Li P, Wang F, Fang W Z, Xu Z, Gao W W and Gao C 2019 Rapid roll-to-roll production of graphene films using intensive Joule heating *Carbon* **155** 462–8

[92] Qiao Y, Chen C J, Liu Y, Liu Y F, Dong Q, Yao Y G, Wang X Z, Shao Y Y, Wang C and Hu L B 2021 Continuous fly-through high-temperature synthesis of nanocatalysts *Nano Lett.* **21** 4517–23

[93] Xiong G W, Jia J, Zhao L L, Liu X Y, Zhang X L, Liu H and Zhou W J 2021 Non-thermal radiation heating synthesis of nanomaterials *Sci. Bull.* **66** 386–406